

This document is confidential and is proprietary to the American Chemical Society and its authors. Do not copy or disclose without written permission. If you have received this item in error, notify the sender and delete all copies.

Stability studies of starch aerogel formulations for biomedical applications

Journal:	<i>Biomacromolecules</i>
Manuscript ID	bm-2020-01414g
Manuscript Type:	Article
Date Submitted by the Author:	01-Oct-2020
Complete List of Authors:	Santos-Rosales, Víctor; Univerity of Santiago de Compostela, Dept Pharmaceutical Technology Alvarez-Rivera, Gerardo; Instituto de Investigacion en Ciencias de la Alimentacion, Laboratory of Foodomics Hillgärtner, Markus; RWTH Aachen University, Department of Continuum Mechanics Cifuentes, Alejandro; Instituto de Investigacion en Ciencias de la Alimentacion, Laboratory of Foodomics Garcia-Gonzalez, C. A.; Univerity of Santiago de Compostela, Dept Pharmaceutical Technology Itskov, Mikhail; Department of Continuum mechanics, Rege, Ameya; German Aerospace Centre, Institute of Materials Research

SCHOLARONE™
Manuscripts

Stability studies of starch aerogel formulations for biomedical applications

*Victor Santos-Rosales¹, Gerardo Alvarez-Rivera², Markus Hillgärtner³, Alejandro Cifuentes²,
Mikhail Itskov³, Carlos A. García-González¹, * and Ameya Rege⁴,***

¹ Department of Pharmacology, Pharmacy and Pharmaceutical Technology, I+D Farma group (GI-1645), Faculty of Pharmacy, Health Research Institute of Santiago de Compostela (IDIS), Agrupación Estratégica de Materiales (AeMAT), Universidade de Santiago de Compostela, E-15782 Santiago de Compostela, Spain.

² Laboratory of Foodomics, Institute of Food Science Research, CIAL, CSIC, Nicolás Cabrera 9, 28049 Madrid, Spain.

³ Department of Continuum Mechanics, RWTH Aachen University, Eilfschornsteinstr. 18, 52062 Aachen, Germany

⁴ Department of Aerogels and Aerogel Composites, Institute of Materials Research, German Aerospace Center (DLR), Linder Höhe, 51147 Cologne, Germany

1
2
3 16 ABSTRACT: Starch aerogels are attractive materials for biomedical applications due to their low
4
5 17 density and high open porosity coupled with high surface areas. However, the lack of
6
7 18 macropores in conventionally-manufactured polysaccharide aerogels is a limitation to their use
8
9 19 as scaffolds for regenerative medicine. Moreover, the stability under storage of polysaccharide
10
11 20 aerogels is critical for biomedical purposes and scarcely studied so far. In this work, the
12
13 21 induction of a new macropore population (1-2 μm) well-integrated in the starch aerogel
14
15 22 backbone was successfully achieved by the incorporation of zein as a porogen. The obtained
16
17 23 dual-porous aerogels were evaluated in terms of composition as well as morphological, textural
18
19 24 and mechanical properties. Stability of aerogels upon storage mimicking the zone II (25 °C, 65 %
20
21 25 relative humidity) according to International Conference on Harmonization (ICH) guideline of
22
23 26 climatic conditions was checked after 1 and 3 months from morphological, physicochemical and
24
25 27 mechanical perspectives. Zein incorporation induced remarkable changes in the mechanical
26
27 28 performance of the end aerogel products and showed a preventive effect on the morphological
28
29 29 changes during the storage period.
30
31
32
33
34
35
36 30
37
38 31
39
40
41
42
43
44
45
46
47
48
49
50
51
52
53
54
55
56
57
58
59
60

32 INTRODUCTION

33 The development of innovative synthetic grafts, known as scaffolds, offers a promising
34 response to regenerate damaged tissues encouraging the self-healing capacity of the patients.
35 Depending on the anatomical target, scaffolds must display a particular 3D interconnected and
36 hierarchical porous structure for an appropriate performance once implanted¹⁻³. Moreover, the
37 mechanical behavior of the grafts is of particular relevance since they should temporarily
38 surrogate the requirements of the natural tissue.

39 Aerogels are solid mesoporous materials characterized by extremely low densities and high
40 open porosities of tailored size and distribution^{5,6}. These properties of aerogels have been widely
41 exploited in several fields, particularly silica and carbon aerogels in the building industries as
42 thermal insulation materials⁷⁻⁹. Nevertheless, bio-based aerogels (i.e. from polysaccharides and
43 proteins) are the mainstream choice for biomedical applications. In particular, starch aerogels
44 emerge as an attractive alternative for bone scaffolds, where the advanced properties of aerogels
45 are supplemented by the biocompatibility, the complete physiological degradation and the
46 abundance of starch in nature¹⁰⁻¹². In addition, starch-based blends promote cell adhesion and
47 proliferation using human osteoblasts^{13,14}.

48 Starch aerogels are formed by a network of intermingled fibers of amylose and amylopectin
49 with a defined micro/mesoporous architecture that can mimic the extracellular matrix.
50 Nevertheless, the usual absence of pores in the macroscale (1 μm and above) hampers the
51 interaction of the scaffold with the biological tissue. The addition of sacrificial porogens (e.g.,
52 salts, sugar or paraffin wax) of defined shapes and dimensions has been explored to confer
53 macroporosity to different aerogel sources¹⁵⁻¹⁸. However, these approaches result in tedious and

1
2
3 54 cumbersome protocols for aerogel processing requiring additional leaching steps to remove the
4
5 55 porogen.
6

7
8 56 Stability studies are mandatory for conventional drug products and medical devices to verify
9
10 57 that raw materials and end products meet the legal requirements in terms of identity, output,
11
12 58 quality and purity over time ¹⁹. Stability in terms of chemical identity, physical form and
13
14 59 biological activity, is a critical parameter that could prevent the clinical use and that gives
15
16 60 practical information to decide on the need and choice of primary and secondary packaging for
17
18 61 the product. However, there is a paucity of information focused on the effect of the storage
19
20 62 period on the performance of nanostructured scaffolds, although those with intricate geometries
21
22 63 are particularly affected by environmental conditions.
23
24

25
26 64 In this work, starch-based aerogels endowed with macroporosity were obtained through an
27
28 65 innovative processing approach involving the use of porogens without extra-leaching steps. Zein,
29
30 66 the major protein of storage of corn, was tested as porogen to induce the formation of well-
31
32 67 integrated macropores in the mesoporous starch aerogel network. The effect of the use of zein
33
34 68 was evaluated on the resulting aerogel composition, textural and mechanical properties. In
35
36 69 addition, quantitative determinations of zein residues in the aerogels were performed, since its
37
38 70 presence favor the *in vivo* promotion of mesenchymal stem cells adhesion and proliferation ^{20,21}.
39
40 71 The stability upon storage was studied on a mid-term (1 and 3 months) mimicking the zone II
41
42 72 International Conference on Harmonization (ICH) guideline of climatic conditions (25 °C, 60 %
43
44 73 relative humidity) ²², which corresponds to the worst case storage scenario for the regions of
45
46 74 Europe, Japan and USA. Scaffolds were monitored in terms of morphological, physicochemical
47
48 75 and mechanical stability.
49
50
51
52
53

54 76

55
56 77 MATERIAL AND METHODS
57
58
59
60

1
2
3 78 **Materials.** Native corn starch (52.6 % amylose content, $\rho_{\text{skel}} = 1.4562 \pm 0.012$ g/mL) was
4
5 79 provided by Roquette Frères S.A. (Lestrem, France). Zein (m.p. 266-283 °C, size of dry
6
7 80 agglomerates by the sieving method: 557 ± 208 μm ; $\rho_{\text{skel}} = 1.167 \pm 0.025$ g/mL) was purchased
8
9 81 from Sigma-Aldrich, Inc. (Madrid, Spain). CO₂ (purity > 99.9 %) was supplied by Praxair, Inc.
10
11 82 (Madrid, Spain). Absolute ethanol (EtOH) was provided by VWR (Radnor, PA, USA).

12
13
14 83 **Corn starch aerogels preparation.** Cylindrical aerogel specimens were obtained by adapting
15
16 84 a previously reported procedure²³. Briefly, starch-aqueous dispersions (10 % w/w) containing
17
18 85 varying ratios of zein as porogen (Table 1) were subjected to a thermal treatment for starch
19
20 86 gelatinization (121 °C, 20 min) and dosed in cylindrical polypropylene molds (length: 14 mm,
21
22 87 diameter: 12 mm). After starch retrogradation at 4 °C for 48 h, the resulting gels were immersed
23
24 88 in absolute ethanol for solvent exchange (gel-alcogel transition) and zein leaching. Solvent was
25
26 89 replaced with fresh ethanol six times at an exchange frequency of 48 h. Starch alcogels were then
27
28 90 loaded in a 100 mL autoclave (Thar Process, Pittsburg, PA, USA) containing 45 mL of absolute
29
30 91 ethanol. A continuous flow of 6 g/min of supercritical CO₂ (40 °C, 130 bar) through the
31
32 92 autoclave during 4 h was employed for ethanol extraction. Subsequently, a controlled
33
34 93 depressurization of 2 bar/min until atmospheric pressure was performed. Aerogel cylindrical
35
36 94 probes (length: *ca.* 11 mm, diameter: *ca.* 8.5 mm) were collected from the autoclave for further
37
38 95 characterization.

39
40 96
41
42 97 **Table 1.** Starch aerogel notation regarding the initial content of starch and zein (expressed in
43
44 98 grams and in weight ratios) used in the batches for the hydrogel formation.

Aerogel	Zein (g)	Starch (g)	Zein-to-starch weight ratio
---------	----------	------------	-----------------------------

Z0	0	8	0:4 (0:1)
Z1	2	8	1:4
Z2	4	8	2:4 (1:2)
Z3	6	8	3:4
Z4	8	8	4:4 (1:1)

99

100

101 **Analytical, physicochemical, structural and mechanical characterization of starch**
 102 **aerogels.** The volume reduction (ΔV , in percentage) of the gels after the solvent exchange and
 103 the supercritical drying steps was evaluated as

$$104 \quad \Delta V = \left(\frac{V_0 - V}{V_0} \right) \times 100 \quad \text{Eq. (1)}$$

105 where V_0 denotes the initial volume of the hydrogel and V the end volume of the alcogel or
 106 aerogel, accordingly.

107 For zein residues quantification in the aerogels, a bottom-up proteomics approach was applied,
 108 involving proteolytic digestion of zein before high-resolution tandem-mass spectrometry
 109 analysis. Starch aerogel samples were dissolved at a concentration of 1 mg/mL in buffer solution
 110 A (10 mM Tris-HCl pH 8.0, 8 M urea) under agitation overnight. Dissolved samples were
 111 diluted in buffer solution B (50 mM Tris-HCl pH 8.0, 0.5 mM CaCl_2) in order to reach urea
 112 concentrations below 6 M. For zein proteins digestion, 370 μL of the previous sample solution
 113 were mixed with 120 μL of thermolysin stock solution prepared in buffer solution B (enzyme-to-
 114 substrate weight ratio 1:20), and incubated for 1 h at 80 °C in an Eppendorf ThermoMixer
 115 (Eppendorf AG, Hamburg, Germany). The digestion reaction was stopped by adding 25 μL of
 116 formic acid (10 vol.%). Digested solutions were filtered through a Microcon-30 kDa Centrifugal
 117 Filter (Merck KGaA, Darmstadt, Germany) before analysis to remove non-digested proteins.

1
2
3 118 An Agilent 1290 UHPLC system coupled to an Agilent 6540 quadrupole-time-of-flight mass
4
5 119 spectrometer (q-TOF MS) and equipped with an orthogonal ESI source was employed for the
6
7 120 determination and quantification of zein residues. Chromatographic separation of digested zein
8
9 121 was conducted using a Zorbax Eclipse Plus C18 column (2.1 × 100 mm, 1.8 μm particle
10
11 122 diameter, Agilent Technologies, Santa Clara, CA, USA) at 30 °C. The mobile phase was
12
13 123 composed of water (0.1 vol.% formic acid, solvent A) and acetonitrile (0.1 vol.% formic acid,
14
15 124 solvent B). A 5-μL aliquot of the sample was injected at a flow rate of 0.5 mL/min during
16
17 125 gradient elution. The gradient program was as follows: 0 min, 0 % B; 7 min, 30 % B; 9 min, 80
18
19 126 % B; 11 min, 100 % B; 13 min, 100 % B; 14 min, 0 % B. The mass spectrometer was operated in
20
21 127 MS and MS/MS modes. MS parameters were the following: capillary voltage, 4000 V; nebulizer
22
23 128 pressure, 40 psi; drying gas flow rate, 10 L/min; gas temperature, 350 °C; skimmer voltage, 45
24
25 129 V; fragmentor voltage, 110 V. The MS and Auto MS/MS modes were set to acquire m/z values
26
27 130 ranging between 50-1100 and 50-800, respectively, at a scan rate of 5 spectra per second.
28
29 131 Operating the ESI source in positive ionization mode, four proteolytic peptides were monitored:
30
31 132 LQQQ (m/z 516.2776), LQQ (m/z 388.2190), FNQ (m/z 408.1877) and FSQ (m/z 381.1768).

32
33 133 Skeletal density of starch aerogels (ρ_{skel}) was determined by helium pycnometry
34
35 134 (Quantachrome, Boynton Beach, FL, USA) at room temperature (25 °C) and 1.01 bar. Values
36
37 135 were obtained from five replicates (standard deviation < 4 %). Bulk density of the aerogels (ρ_{bulk})
38
39 136 was determined by weighing and measuring their dimensions. The resulting overall porosity (ϵ)
40
41 137 and total pore volume were calculated from Eqs. (2) and (3), respectively.

42
43 138
$$\epsilon = \left(1 - \frac{\rho_{bulk}}{\rho_{skel}}\right) \times 100 \quad \text{Eq. (2)}$$

44
45 139
$$V_p = \left(\frac{1}{\rho_{bulk}} - \frac{1}{\rho_{skel}}\right) \quad \text{Eq. (3)}$$

1
2
3 140 Textural properties of the aerogels were determined by N₂ adsorption-desorption analyses
4
5 141 (ASAP 2000 Micromeritics Inc, Norcross, GA, USA). Prior to the measurements, aerogels were
6
7 142 outgassed at 80 °C and under vacuum (<1 mPa) for 24 h. Specific surface area (A_{BET}) of the
8
9 143 aerogels scaffolds were determined by the Brunauer-Emmett-Teller (BET) method. Specific pore
10
11 144 volumes ($V_{\text{p,BJH}}$) and mean pore diameter ($d_{\text{p,BJH}}$) were evaluated from the desorption branch of
12
13 145 the isotherms using the Barrett-Joyner-Halenda (BJH) method (Figure S1).
14
15

16
17 146 Based on the BJH-pore volume distribution, the contributions (in percentage) of mesopores (2-
18
19 147 50 nm range, $V_{\text{p,meso}}$) to the total pore volume were determined. The contribution of the
20
21 148 macropore population (>50 nm, $V_{\text{p,macro}}$) was determined by the difference between the total
22
23 149 specific pore volume and the specific mesopore volume ($V_{\text{p,meso}}$).
24
25

26 150 The structure of the aerogels was evaluated by scanning electron microscopy (FESEM,
27
28 151 ULTRA-PLUS, Zeiss, Oberkochen, Germany) running at 3 kV. Prior to imaging, aerogels were
29
30 152 sputtered with a layer of iridium of 10 nm thickness.
31
32

33 153 The mechanical behavior of cylindrical aerogel specimens was analyzed by means of uniaxial
34
35 154 quasistatic compression tests using a 10 kN load cell on the universal testing machine Z010
36
37 155 (Zwick/Roell GmbH, Ulm, Germany). The strain rate of 10 %/min was applied for all
38
39 156 compression tests. To characterize the inelastic features of the aerogels, cyclic compression was
40
41 157 conducted, whereby the aerogel specimens were subjected to three sets of loading and unloading
42
43 158 cycles with the strain amplitude increased stepwise by 20 %. All the experiments were
44
45 159 performed at 20 °C, atmospheric pressure and in triplicate.
46
47
48

49 160
50
51 161 **Stability tests under storage of starch aerogels.** Aerogel cylindrical probes of each
52
53 162 composition were placed inside sterile glass vessels with hermetic closure, containing a solution
54
55
56
57
58
59
60

1
2
3 163 of sulfuric acid (37 % v/v) to maintain the relative humidity at 65 %²⁴. Containers were stored
4
5 164 for either 1 or 3 months at 25 °C. After the storage time was elapsed, aerogels were collected for
6
7
8 165 their complete characterization-

9
10 166 **Statistical analysis.** All results were expressed as mean \pm standard deviation. Statistical
11
12 167 analyses of shrinkage values (1-way ANOVA) were performed followed by the post hoc Tukey-
13
14
15 168 Kramer method test using Statistica v.8.0 software (StatSoft Inc., Tulsa, OK, USA)

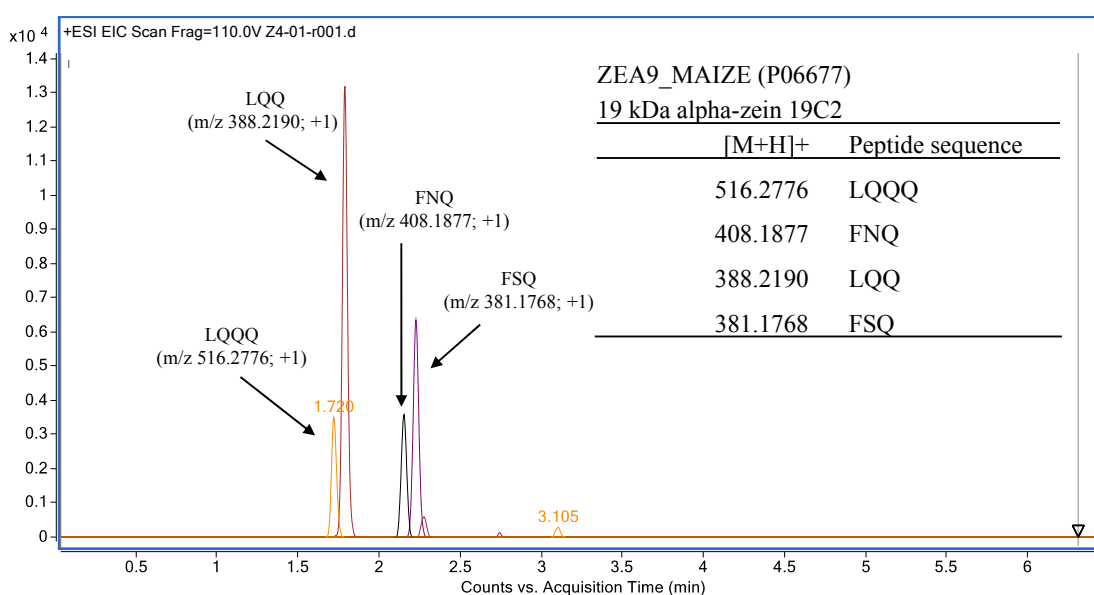
16
17 169

18 19 170 RESULTS AND DISCUSSION

20
21 171 **Morphological and physicochemical characterization of starch-based macroporous**
22
23
24 172 **aerogels.** Corn starch aerogels were prepared in the form of cylindrical monoliths for a
25
26 173 reproducible determination of their densities and mechanical properties. White solid lightweight
27
28 174 structures were obtained in all cases, although the modified starch aerogels showed a slight
29
30
31 175 yellow coloration suggesting the presence of zein residues (Figure S2). The use of zein favored
32
33 176 the homogeneous dosing of the aqueous dispersion in the moulds. The reduced content of
34
35 177 amylose in the admixture extended its retrogradation rate since less intermolecular hydrogen-
36
37
38 178 bondings were formed within the dispersion^{11,25}.

39
40 179 A determination method based on a bottom-up approach was set up to quantify zein residues in
41
42 180 the aerogel samples. The full sequence of 19 kDa alpha-zein 19C2 (ZEA9 MAIZE – P06677)
43
44 181 protein was obtained from Uniport database, and the whole sequence of peptides was exported to
45
46
47 182 PeptideMass tool from ExPasy website for *in silico* digestion. Theoretical peptide masses of the
48
49 183 input proteins were generated applying the following stringent criteria: thermolysin was selected
50
51 184 as digestion enzyme, and only one missed cleavage was allowed for thermolysin digestion.

1
2
3 185 Operating the HPLC-ESI-QTOF system in the positive ionization mode (ESI+), a targeted
4
5 186 screening analysis in full MS mode (m/z 100–1100 mass range) was performed to identify the
6
7 187 m/z $[M+H]^+$ peptide masses obtained from *in silico* digestion in a zein standard solution and in
8
9 188 the starch aerogel sample theoretically containing the highest zein content (Z4). Figure 1 shows
10
11 189 four selected zein peptides masses ($m/z = 516.2776$ $[LQQQ+H]^+$; 388.2190 $[LQQ+H]^+$; 408.1877
12
13 190 $[FNQ +H]^+$; 381.1768 $[FSQ +H]^+$) in Z4 sample. These peptides were selected for zein
14
15 191 determination, exhibiting satisfactory intensity, sensitivity and dynamic range.
16
17
18



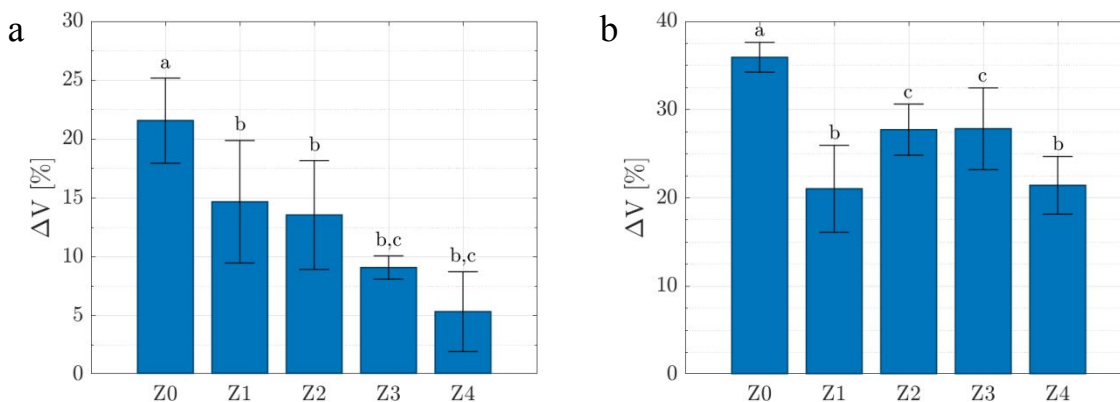
192
193 **Figure 1.** High-resolution extracted ion chromatograms (HREICs) of Z4 starch aerogel, showing
194 the target peptides masses (10 ppm extraction window) for zein residues determination in
195 aerogels.

196 Table 2 shows the main LC-HRMS parameters for the target peptides, including
197 chromatographic retention time, monoisotopic mass, protonated molecular ion and calculated
198 mass error ($\Delta m/z$). The identification of zein peptides was based on identity of the exact mass,
199 monoisotopic profile and MS/MS fragmentation spectra (Figure S3). Zein content in Z0-Z4

200 starch aerogels was determined by external standard calibration using a zein standard solution
 201 submitted to the same digestion process as the starch samples (see Table 2).
 202
 203 **Table 2.** HPLC-HRMS parameters of target zein peptide fragment. Concentration values (%
 204 w/w) for zein residues in different starch aerogels.

RT (min)	Peptide sequence	Formula	Monoisot opic mass	[M+H] ⁺ (m/z)	Error (ppm)	Concentration in starch (% w/w ± std)				
						Z0	Z1	Z2	Z3	Z4
1.719	LQQ Q	C ₂₁ H ₃₇ N ₇ O ₈	515.2704	516.2776	1.0	nd	4.0±0.1	13.5±0.1	12.8±1.1	27.4±0.9
1.795	LQQ	C ₁₆ H ₂₉ N ₅ O ₆	387.2118	388.2190	3.6	nd	3.3±0.1	9.9±0.2	10.4±0.3	21.2±0.2
2.153	FNQ	C ₁₈ H ₂₅ N ₅ O ₆	407.1805	408.1877	1.5	nd	3.8±0.1	11.3±0.7	12.3±1.0	25.5±0.2
2.229	FSQ	C ₁₇ H ₂₄ N ₄ O ₆	380.1696	381.1768	4.2	nd	3.7±0.4	7.2 ±0.5	11.1±1.1	21.1±0.9
Average zein concentration						nd	3.7±0.3	10.5± 2.6	11.6±1.1	23.8±3.1

205
 206 All the manufactured starch aerogels had a certain volume shrinkage mainly during the solvent
 207 exchange step and, in a lesser extent, during the supercritical drying step (Figure 2). The addition
 208 of the zein in the aerogels strongly reduced the shrinkage values, particularly during gel-alcogel
 209 transition. For instance, a 4-fold reduction in these values was observed for Z4 aerogels.
 210 However, this effect was not linear and aerogels with similar residual zein content (Z2, Z3, in
 211 Table 2) behaved differently. On the other hand, the volume reduction detected during the
 212 supercritical drying was severe, although the overall shrinkage values are in accordance with
 213 those reported for starch aerogels with similar amylose contents (30-40 %) ^{26,27}. Interestingly, Z1
 214 aerogels presented similar values to Z4, despite of the fact that zein residues were much higher in
 215 the latter formulation.



216 **Figure 2.** Volume shrinkage of starch-based gels after (a) the solvent exchange and (b)
 217 supercritical drying. Equal letters denote statistically homogeneous groups.

218 Bulk densities of the obtained aerogels (ρ_{bulk}) strongly depended on the initial hydrogel
 219 composition (Table 3). Aerogel formulations prepared from hydrogels with lower zein contents
 220 (Z1, Z2) were significantly lighter (*ca.* 30%) than pure starch aerogels (Z0) ($p > 0.05$).
 221 Conversely, denser structures were proportionally obtained with zein content when the 1:2 zein-
 222 to-starch weight ratio was exceeded for the Z2-Z3-Z4 aerogel sequence. The remaining zein
 223 residues are responsible for this effect as depicted in Table 2. For example, Z3 presented almost
 224 identical density values to the unmodified formulations (Z0), whereas Z4 aerogels were the
 225 heaviest structures. Accordingly, the overall porosity of the aerogels (ε) followed a reverse trend
 226 with respect to the bulk density, but falling in the 85-91 % range in all cases, which is
 227 advantageous for regenerative medicine applications as scaffold matrices²⁸.

228 The technical feasibility of the processing strategy to induce a larger pore population in starch
 229 aerogels was confirmed from the textural analysis (Table 3). The zein addition in the aerogel
 230 formulations resulted in increased specific surface areas ($A_{\text{BET}} = 183\text{-}228 \text{ m}^2/\text{g}$) with values in
 231 the range of those reported for high amylose corn starch aerogels^{12,26,29}. Similarly, the specific
 232 pore volume ($V_{\text{p,BJH}}$) was higher as the porogen content increased while the mean pore diameter

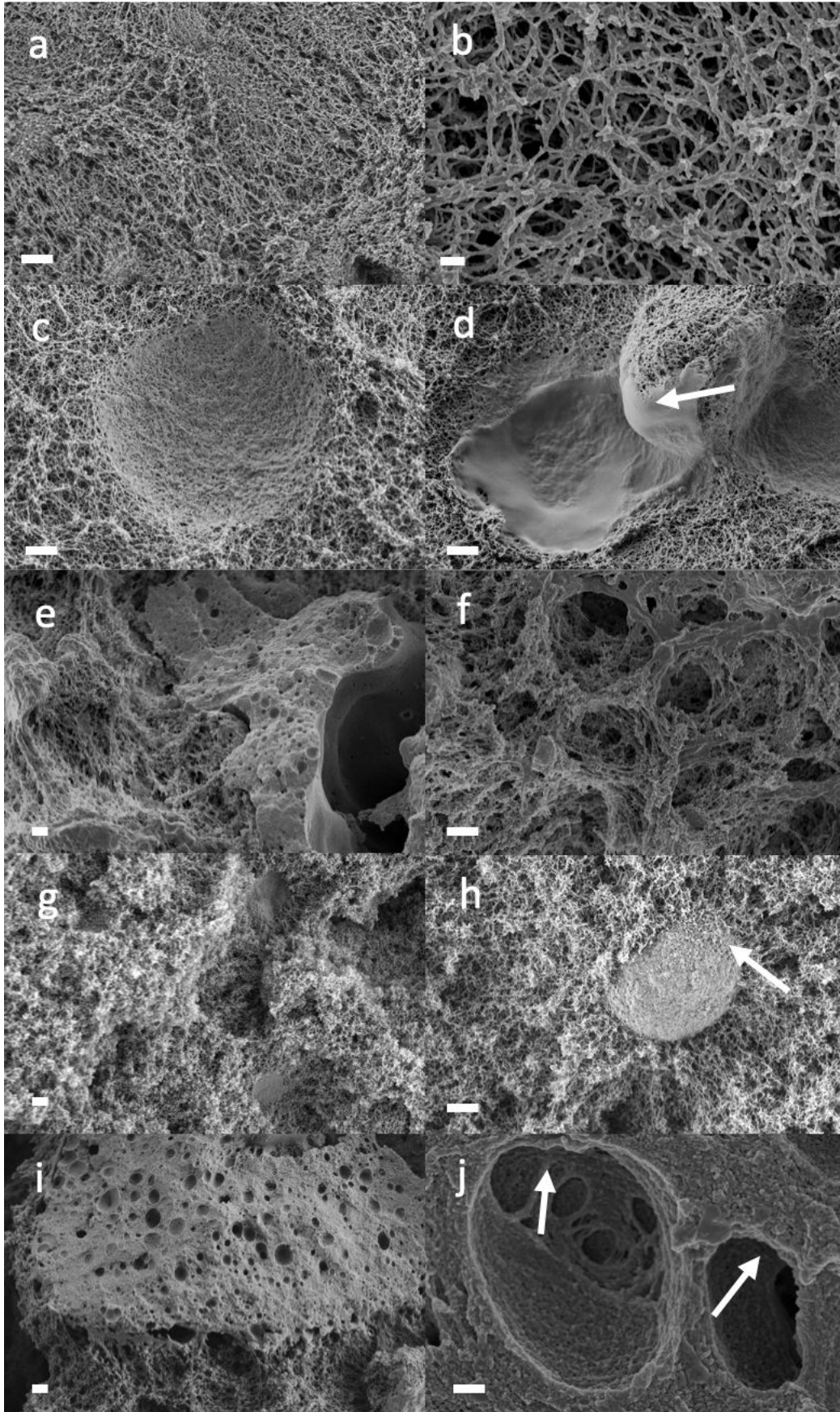
1
2
3 233 ($d_{p,BJH}$) remained constant at 18-20 nm. The formation of dual porous aerogels was confirmed
4
5 234 from the macropore contribution to the overall porous values ($V_{p,macro}$ in Table 3). The total pore
6
7 235 volume and macropore contribution were determined by the combination of N_2 adsorption-
8
9 236 desorption and helium pycnometry analyses, since the contribution of macropores in the pore
10
11 237 volume (over 80 % of the overall porosity for other bio-aerogels^{30,31}), may not be taken into
12
13 238 account in the characterization of aerogels through the BJH method. The zein effect in
14
15 239 macropore formation is clearly appreciated from Z0 to Z2 aerogels by an increase in $V_{p,macro}$ of
16
17 240 up to 4 %. Conversely, $V_{p,macro}$ values for Z3 and Z4 aerogels were similar and 10 % lower than
18
19 241 that ones for unmodified aerogels (Z0). Although most of the porogen was leached during the
20
21 242 solvent exchange step, the zein residue of 10 to 20 wt.% quantified in the abovementioned
22
23 243 formulations is responsible for their densification and thus directly decreasing the pore volume
24
25 244 V_p since it is a specific parameter (i.e. expressed in a mass basis). (Table 3).

26
27 245 Scanning electron microscopy (SEM) images of starch aerogels confirmed that their
28
29 246 morphology and texture were dramatically influenced by the presence of zein porogen in the
30
31 247 aerogel processing (Figure 3). The unmodified aerogel (Z0) presented an interconnected fiber
32
33 248 network in the 30-60 nm diameter range (Figures 3a,b) typical for starch aerogels³². The
34
35 249 incorporation of zein during the aerogel processing induced remarkable morphological changes
36
37 250 to the aerogel architectures with the presence of spherical macropores (*ca.* 2 μ m) even in the
38
39 251 formulation with lower zein content (Z1 in Figures 3c,d). This new pore family presented inner
40
41 252 rough surfaces, but the presence of a thin film in certain pores (Figure 3d) suggested an
42
43 253 incomplete zein removal during the solvent exchange step. The observed morphology was thus
44
45 254 coherent with the zein quantifications (Table 2). The thermal treatment for the starch
46
47 255 gelatinization disrupts the close-packed tertiary globular structure of zein, increasing its water
48
49
50
51
52
53
54
55
56
57
58
59
60

1
2
3 256 soluble fraction and promoting the formation of disulphide bonds³³⁻³⁵. Therefore, the formation
4
5 257 of zein agglomerates are favored due to the higher interactions between polypeptide chains^{36,37}.
6
7 258 Z2 aerogels presented regions of large protein aggregates (>10 μm) and also regions of perfectly
8
9 259 integrated dual and interconnected porosity (Figures 3e,f). Aerogels prepared with higher
10
11 260 contents of porogen led to more irregular structures (Z3 in Figures 3g,h, and Z4 in Figures 3i,j),
12
13 261 supporting the increased specific surface areas values (A_{BET} in Table 3). The formation of larger
14
15 262 pores in Z3 aerogels was clearly identified as the footprint of zein particles after the leaching
16
17 263 (Figure 3g). The remaining globular zein residues embedded in the starch mesoporous backbone
18
19 264 were also observed (Figure 3h). The presence of porous zein films was more abundant in Z4
20
21 265 formulation (Figure 3i). Overall, the formation of a family of large (1-3 μm) and interconnected
22
23 266 macropores was achieved through the use of zein as porogen (Figure 3j).
24
25
26
27
28
29
30
31
32
33
34
35
36
37
38
39
40
41
42
43
44
45
46
47
48
49
50
51
52
53
54
55
56
57
58
59
60

Table 3. Morphological and textural properties of the obtained aerogels. Values expressed as mean values and standard deviation.

Aerogel	ρ_{bulk} (g/mL)	ρ_{skel} (g/mL)	ε (%)	A_{BET} (m ² /g)	$V_{p,BJH}$ (cm ³ /g)	$d_{p,BJH}$ (nm)	V_p (cm ³ /g)	$V_{p,meso}$ (%)	$V_{p,macro}$ (%)	
Z0	<i>No storage</i>	0.175 ± 0.004	1.478 ± 0.05	88.1 ± 0.4	183 ± 9	1.01 ± 0.05	19.1 ± 1.0	5.03	15.1	84.9
	<i>1 month</i>	0.200 ± 0.005	1.495 ± 0.03	86.6 ± 0.4	217 ± 11	1.30 ± 0.07	21.6 ± 1.1	4.33	20.8	79.2
	<i>3 months</i>	0.184 ± 0.006	1.467 ± 0.03	87.5 ± 0.4	213 ± 11	1.30 ± 0.06	23.3 ± 1.2	4.76	18.6	81.4
Z1	<i>No storage</i>	0.120 ± 0.013	1.349 ± 0.02	91.1 ± 1.0	228 ± 11	1.29 ± 0.06	18.9 ± 0.9	7.57	12.7	87.3
	<i>1 month</i>	0.158 ± 0.005	1.389 ± 0.04	88.6 ± 0.5	226 ± 11	1.07 ± 0.05	16.9 ± 0.8	5.59	13.8	86.2
	<i>3 months</i>	0.150 ± 0.006	1.414 ± 0.05	89.4 ± 0.5	85 ± 4	0.43 ± 0.02	18.4 ± 0.9	5.94	4.9	95.1
Z2	<i>No storage</i>	0.120 ± 0.006	1.465 ± 0.01	91.8 ± 0.4	226 ± 11	1.25 ± 0.06	19.0 ± 1.0	7.62	11.0	89.0
	<i>1 month</i>	0.134 ± 0.009	1.394 ± 0.03	90.4 ± 0.7	164 ± 8	0.87 ± 0.04	18.0 ± 0.9	6.76	8.6	91.4
	<i>3 months</i>	0.135 ± 0.006	1.433 ± 0.04	90.6 ± 0.5	120 ± 6	0.60 ± 0.03	16.5 ± 0.8	6.69	6.4	93.6
Z3	<i>No storage</i>	0.172 ± 0.006	1.385 ± 0.02	87.6 ± 0.5	204 ± 10	1.18 ± 0.06	19.9 ± 1.0	5.08	16.0	84.0
	<i>1 month</i>	0.182 ± 0.006	1.369 ± 0.03	86.7 ± 0.5	184 ± 9	0.97 ± 0.05	17.3 ± 0.9	4.78	14.5	85.5
	<i>3 months</i>	0.176 ± 0.007	1.360 ± 0.01	87.0 ± 0.5	178 ± 9	0.98 ± 0.05	17.8 ± 0.9	4.93	15.1	84.9
Z4	<i>No storage</i>	0.192 ± 0.016	1.353 ± 0.02	85.8 ± 1.2	226 ± 11	1.35 ± 0.07	19.0 ± 0.9	4.46	22.5	77.5
	<i>1 month</i>	0.197 ± 0.002	1.350 ± 0.03	85.4 ± 0.4	207 ± 10	1.30 ± 0.07	21.2 ± 1.1	4.35	20.1	79.9
	<i>3 months</i>	0.187 ± 0.008	1.303 ± 0.03	85.6 ± 0.7	157 ± 8	0.91 ± 0.05	19.0 ± 0.9	4.58	15.1	84.9



1
2
3 **Figure 3.** SEM images of horizontal cross-sections of the obtained starch-based aerogels. (a,b)
4 Characteristic microstructure of unmodified aerogels (Z0). (c,d) The addition of low contents of
5 the porogen (Z1) and later leaching induced the formation of larger pores with rough inner
6 surfaces, although thin films of zein residues could be observed along the aerogel (d, arrow).
7
8 (e,f) More residues were detected for Z2 in certain areas, but an interconnected porous network
9 was obtained. (g,h) The incorporation of higher zein amounts (Z3) leads to more irregular
10 surfaces and entire spherical zein particles were identified (h, arrow), highlighting the
11 uncompleted porogen leaching. (i,j) Z4 aerogel formulation presented numerous porous zein
12 plates well-integrated with the starch network backbone. (j) In addition, larger and
13 interconnected pores (arrows) with noticeable roughness were obtained. Scale bars: 300 nm (b, j)
14 and 2 μm (a, c-i).

15
16
17
18
19
20
21
22
23
24
25
26
27
28
29 **Mechanical characterization of starch aerogels.** All starch aerogel formulations were
30 subjected to uniaxial quasistatic compressions of up to 70 % strain (Figure 4). The mechanical
31 response of the aerogels showed an irregular nature subject to addition of the zein component.
32 Considering the pure starch aerogel (Z0) as the reference, the curves corresponding to Z1 and Z2
33 showed that the addition of zein strongly softened their stress-strain response. This behavior is
34 clearly related to the formation of hollow spaces in the starch aerogel backbone (Figure 3).
35 However, this softening trend was reversed for the case of the aerogels with higher zein residues
36 (Z3, Z4 in Table 2) and its stiffness was strongly enhanced. For instance, the stiffness of the
37 starch aerogel processed with the highest zein content (Z4) was even stronger than the reference
38 aerogel Z0. The compression moduli of the five aerogel formulations are illustrated in Figure 4
39 to quantitatively show this effect. A polynomial fit expressing the relation between Young's
40 modulus under compression (given in MPa) and the zein-to-starch ratio is expressed as follows
41
42
43
44
45
46
47
48
49
50
51
52
53
54
55
56
57
58
59
60

$$E(c) = -4.2157c^3 + 12.1715c^2 - 7.1856c + 2.0639 \quad \text{Eq (4)}$$

where $c \in [0,1]$ denotes the zein-to-starch weight ratio. For the aerogels in consideration, an explanation to the trend seen in Figure 5 can be deduced from the bulk density measurements in Table 3. Porous materials, such as aerogels, exhibit a power-law scaling relation between Young's modulus E and the bulk density (ρ_{bulk})^{38–40}. Such scaling behavior is also specifically observed in other polysaccharide-based aerogels^{41–45}. Table 3 shows the effect of zein on the bulk densities of the aerogels, where a decreasing trend from Z0→Z1→Z2 and an increasing trend from Z2→Z3→Z4 were observed. This explains the trend of Young's modulus vs. the zein-to-starch weight ratio (density) curve. The addition of zein as a porogen induced the formation of macropores, which also influenced the overall macroscopic mechanical behavior of the aerogels. Such influence of the hierarchical porous structure on the mechanical behavior was previously reported for cellulose aerogels⁴⁶.

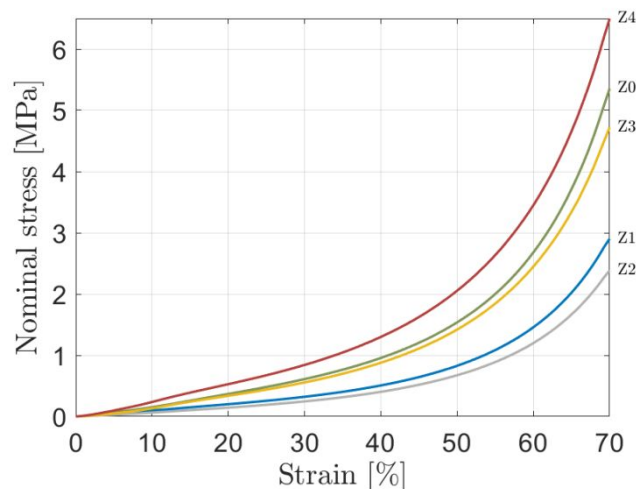


Figure 4. Stress-strain curves of starch aerogels processed with different zein contents (Z0 to Z4 with increasing zein content) tested under compression.

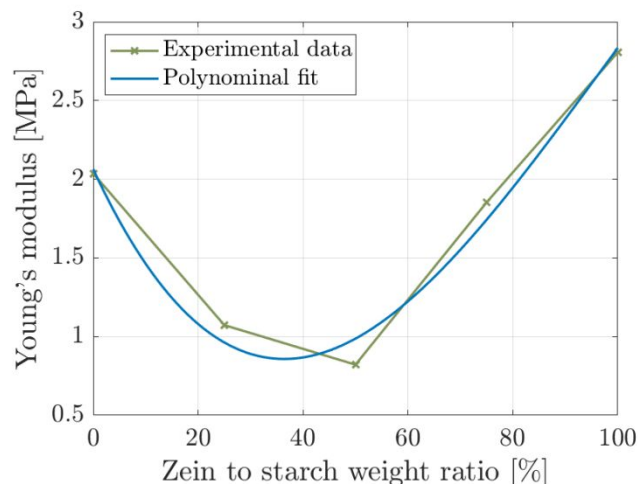


Figure 5. Effect of the zein content used during the starch aerogel processing on Young's moduli of the aerogels. A polynomial fit is generated to show the relation between the zein-to-starch weight ratio (in percentage, adhering to Eq. (4)) to Young's modulus.

Under cyclic loading, all the tested aerogels show typical elastoplastic behavior, with very large permanent set (Figures 6 and S4). This behavior is typical of other biopolymer-based aerogels⁴³. The very small hysteresis (area between the unloading curve of a cycle and the reloading curve of the subsequent cycle) along with the permanent set indicate severe irreversible damage within the microstructure of the aerogel network. However, the aerogels exhibit a good strain memory as the reloading curve comes back to the point of the maximal strain of the previous loading cycle and continues the path as if it were the monotonic loading (Figure 6).

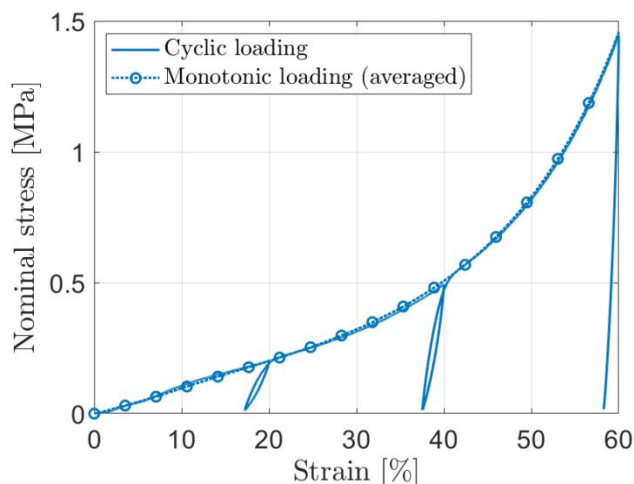


Figure 6. Stress-strain response of Z1 aerogels under cyclic loading-unloading quasistatic compression. The specimen was subjected to three sets of loading cycles with the strain amplitude increased stepwise by 20 %. The monotonic loading curve is illustrated as a dotted line, demonstrating a memory of the aerogels. Curves of the other tested formulations (Z0, Z2, Z3 and Z4) showed a similar behavior and can be found as supplementary material (Figure S4).

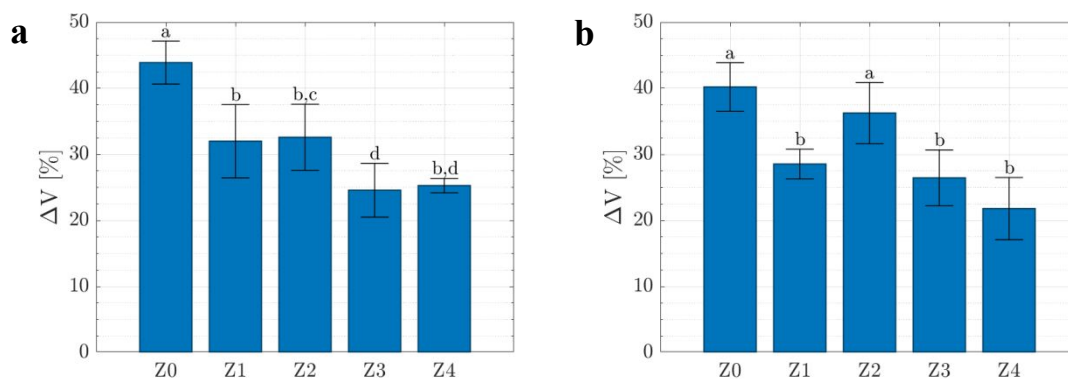
Effect of storage time. The stability under storage of drug products, medical devices and combination products (i.e. products comprising a drug and a medical device, or a biological product and a medical device) is a critical quality parameter within a well-established legal framework, since the variety of degradation processes (chemical, physical, biopharmaceutical) that may occur could render products ineffective or unsafe before patient use²². Nevertheless, there is paucity of information on research regarding the stability of complex porous architectures conceived as scaffolds⁴⁷.

The exposition to the storage conditions induced certain volume shrinkage of the starch aerogels. Formulations containing higher zein residues (Z3, Z4) presented values identical to their non-stored counterparts, thus preserving their initial structure. On the other hand, higher

1
2
3 volume shrinkages close to 5 % were observed for unmodified aerogels (Z0) after 3 months of
4 storage (Figure 7).
5
6

7
8 After 1 month of storage at 25 °C and 65 % relative humidity, aerogels experienced a
9 densification in the 3-32 % range, depending on the formulation (Table 3). The highest
10 densification was reached for Z1 aerogel, whereas this effect was very low in formulations with
11 higher initial zein-to-starch weight ratio (Z2-Z4). This preventive effect can be directly attributed
12 to the zein residues (Table 2).
13
14
15
16
17
18

19 Interestingly, bulk densities of aerogels after 3 months were lower than after 1 month,
20 regardless the aerogel composition. The incorporation of higher amounts of zein reduced the
21 storage impact, obtaining slightly lighter structures for Z4 after 3 months of storage. Overall, all
22 manufactured aerogels experienced a densification and a mild reduction in the overall porosity
23 after the storage period (Table 3).
24
25
26
27
28
29
30



44 **Figure 7.** Overall shrinkage values of starch aerogels after the storage periods of (a) 1 month and
45 (b) 3 months. Equal letters denote statistically homogeneous groups.
46
47
48

49
50 The densification of the aerogels after the storage had a parallel impact on the textural
51 properties, with consistent decreases in the specific surface areas (A_{BET} in Table 3). Aerogel
52 formulations containing zein presented a reduction in the $V_{\text{p,BJH}}$ values. This is attributed to the
53
54
55
56
57
58
59
60

1
2
3 swelling ability of amylopectin in humid environment that would cause the pore collapse, mainly
4 affecting the smaller pore population ⁴⁸. In general, the impact of storage on the aerogel
5 formulations depended on the remaining porogen traces. In Z1 and Z2, the major part of the zein
6 was leached during the aerogel processing, leading to a more open structure and thus favoring
7 the water intake, as suggested by both the remarkable decrease in $V_{p, \text{BJH}}$ and the increase in the
8 $V_{p, \text{macro}}$ values. The presence of hydrophobic zein residues along the aerogel monoliths may
9 hinder the starch interaction with the moisture ⁴⁹. Accordingly, Z3 and Z4 aerogels had less
10 drastic variations in the textural properties. For instance, $V_{p, \text{macro}}$ of Z3 aerogels after 3 months of
11 storage was nearly identical to its non-stored counterpart.

12
13
14
15
16
17
18
19
20
21
22
23
24 After the storage period (1 and 3 months), aerogels were tested again under quasistatic
25 compression. Despite the abovementioned morphological changes mainly in the smaller pore
26 population (micropores), their mechanical performance was virtually unaffected after the storage
27 period under 25 °C and 65 % relative humidity (Figure 8). In previous theoretical studies on
28 modeling of biopolymer aerogels ^{40,50}, it was proposed that pores (cellular fiber-network) within
29 the microporous region and lower mesoporous region do not play a significant role in the overall
30 mechanical performance of the aerogels. This could explain the absence of an effect on the
31 stress-strain response due to a reduction in the amount of micropores and lower mesopores. The
32 result illustrated in Figure 8 opens up questions that need further investigations by theoretical
33 and experimental approaches. The stored aerogels were further subjected to cyclic loading and
34 showed similar elastoplastic behavior as that of the non-stored aerogels:-
35
36
37
38
39
40
41
42
43
44
45
46
47
48
49
50
51
52
53
54
55
56
57
58
59
60

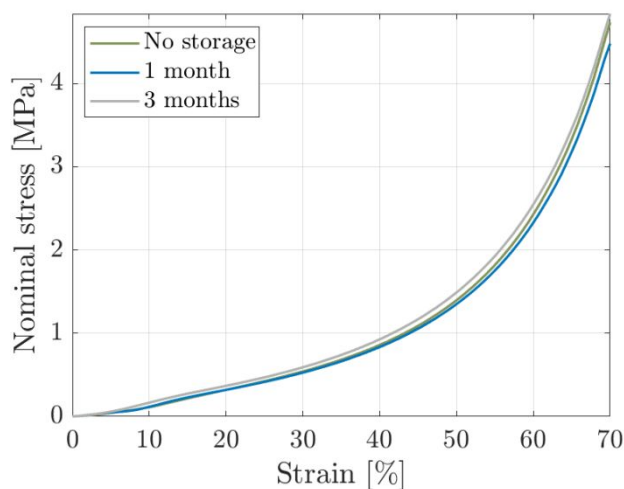


Figure 8. Uniaxial quasistatic compression curves of starch aerogel (Z3) specimens subject to different storage duration (0, 1 and 3 months) at 25 °C and 65 % relative humidity. Curves for the rest of aerogels can be found in the supplementary information (Figure S5).

CONCLUSIONS

Starch aerogels displaying a new macropore population (1-2 μm) were successfully manufactured by the incorporation of zein as a porogen. Highly porous aerogels (85-92 %) were obtained with well-integrated macropores in the mesoporous starch aerogel backbone, encouraging its use as scaffolds for tissue engineering applications. Zein incorporation induced remarkable changes in the mechanical performance of the end aerogel products with an enhanced stiffness. The storage period mimicking the ICH-climatic conditions of Europe, USA and Japan induced morphological modifications in the aerogels whilst the mechanical behavior was virtually unaffected. The presence of zein residues along the aerogel scaffolds had a preventive effect on the morphological changes during the storage period. Overall, zein appears as an advantageous biocompatible porogen for the processing of dual-porous starch aerogels from the

1
2
3 technological (integration in classical aerogel processing pathway without extra-leaching steps)
4
5 and materials performance (enhanced stiffness and stability) points of view.
6
7
8
9

10 ASSOCIATED CONTENT

11
12
13
14 **Supporting Information.** Pore size distributions from BJH-desorption, physical appearance of
15 aerogel, HPLC-QTOF-MS/MS fragmentation spectra of target peptides, compressive behavior of
16 starch aerogel composites under cyclic loading and different storage time periods.
17
18
19

20 AUTHOR INFORMATION

21 **Corresponding Authors**

22
23
24
25
26
27 * Carlos A. García-González. [*carlos.garcia@usc.es](mailto:carlos.garcia@usc.es), Tel.: +34-881-814882
28
29

30
31 ** Ameya Rege. [**ameya.rege@dlr.de](mailto:ameya.rege@dlr.de), Tel.: +49-2203-6015158
32
33

34 **Author Contributions**

35
36 The manuscript was written through contributions of all authors. All authors have given approval
37 to the final version of the manuscript.
38
39

40 **Notes**

41
42 The authors declare no competing financial interest.
43
44
45
46
47
48
49

50 ACKNOWLEDGEMENTS

1
2
3 This research was funded by Xunta de Galicia [ED431F 2016/010; ED431C 2020/17],
4 MCIUN [RTI2018-094131-A-I00], Agrupación Estratégica de Materiales [AeMAT-
5 BIOMEDCO2, ED431E 2018/08], Agencia Estatal de Investigación [AEI] and FEDER funds. V.
6 Santos-Rosales acknowledges to Xunta de Galicia (Consellería de Cultura, Educación e
7 Ordenación Universitaria) for a predoctoral research fellowship [ED481A-2018/014]. C.A.
8 García-González acknowledges to MINECO for a Ramón y Cajal Fellowship [RYC2014-
9 15239]. Authors would like to thank Roquette (Spain) for kindly providing the starch and to
10 Plataforma Proteómica-Metabólica (CEI-UAM+CSIC) for the zein analysis. Work carried out
11 in the frame of the COST Action CA18125 “Advanced Engineering and Research of aeroGels
12 for Environment and Life Sciences” (AERoGELS) and funded by the European Commission.
13
14
15
16
17
18
19
20
21
22
23
24
25
26
27
28

29 REFERENCES

- 30
31
32 (1) Jafari, M.; Paknejad, Z.; Rad, M. R.; Motamedian, S. R.; Eghbal, M. J.; Nadjmi, N.;
33 Khojasteh, A. Polymeric Scaffolds in Tissue Engineering: A Literature Review: Polymeric
34 Scaffolds in Tissue Engineering. *Journal of Biomedical Materials Research Part B: Applied*
35 *Biomaterials* **2017**, *105* (2), 431–459. <https://doi.org/10.1002/jbm.b.33547>.
36
37
38
39
40
41
42 (2) Loh, Q. L.; Choong, C. Three-Dimensional Scaffolds for Tissue Engineering
43 Applications: Role of Porosity and Pore Size. *Tissue Engineering Part B: Reviews* **2013**, *19* (6),
44 485–502. <https://doi.org/10.1089/ten.teb.2012.0437>.
45
46
47
48
49
50 (3) Santos-Rosales, V.; Iglesias-Mejuto, A.; García-González, C. A. Solvent-Free
51 Approaches for the Processing of Scaffolds in Regenerative Medicine. *Polymers* **2020**, *12* (3),
52 533. <https://doi.org/10.3390/polym12030533>.
53
54
55
56
57
58
59
60

1
2
3 (4) García-González, C. A.; Concheiro, A.; Alvarez-Lorenzo, C. Processing of Materials for
4 Regenerative Medicine Using Supercritical Fluid Technology. *Bioconjugate Chem.* **2015**, *26* (7),
5 1159–1171. <https://doi.org/10.1021/bc5005922>.
6
7

8
9
10 (5) Maleki, H.; Durães, L.; García-González, C. A.; del Gaudio, P.; Portugal, A.; Mahmoudi,
11 M. Synthesis and Biomedical Applications of Aerogels: Possibilities and Challenges. *Advances*
12 *in Colloid and Interface Science* **2016**, *236*, 1–27. <https://doi.org/10.1016/j.cis.2016.05.011>.
13
14
15

16 (6) Ganesan, K.; Budtova, T.; Ratke, L.; Gurikov, P.; Baudron, V.; Preibisch, I.; Niemeyer,
17 P.; Smirnova, I.; Milow, B. Review on the Production of Polysaccharide Aerogel Particles.
18 *Materials* **2018**, *11* (11), 2144. <https://doi.org/10.3390/ma11112144>.
19
20
21
22

23 (7) Randall, J. P.; Meador, M. A. B.; Jana, S. C. Tailoring Mechanical Properties of Aerogels
24 for Aerospace Applications. *ACS Applied Materials & Interfaces* **2011**, *3* (3), 613–626.
25 <https://doi.org/10.1021/am200007n>.
26
27
28

29 (8) Koebel, M.; Rigacci, A.; Achard, P. Aerogel-Based Thermal Superinsulation: An
30 Overview. *Journal of Sol-Gel Science and Technology* **2012**, *63* (3), 315–339.
31 <https://doi.org/10.1007/s10971-012-2792-9>.
32
33

34 (9) García-González, C. A.; Budtova, T.; Durães, L.; Erkey, C.; Del Gaudio, P.; Gurikov, P.;
35 Koebel, M.; Liebner, F.; Neagu, M.; Smirnova, I. An Opinion Paper on Aerogels for Biomedical
36 and Environmental Applications. *Molecules* **2019**, *24* (9), 1815.
37 <https://doi.org/10.3390/molecules24091815>.
38
39
40

41 (10) Zhu, F. Starch Based Aerogels: Production, Properties and Applications. *Trends in Food*
42 *Science & Technology* **2019**, *89*, 1–10. <https://doi.org/10.1016/j.tifs.2019.05.001>.
43
44
45
46
47
48
49
50

1
2
3 (11) García-González, C. A.; Alnaief, M.; Smirnova, I. Polysaccharide-Based Aerogels—
4 Promising Biodegradable Carriers for Drug Delivery Systems. *Carbohydrate Polymers* **2011**, *86*
5
6 (4), 1425–1438. <https://doi.org/10.1016/j.carbpol.2011.06.066>.
7
8

9
10 (12) Mehling, T.; Smirnova, I.; Guenther, U.; Neubert, R. H. H. Polysaccharide-Based
11 Aerogels as Drug Carriers. *Journal of Non-Crystalline Solids* **2009**, *355* (50–51), 2472–2479.
12
13 <https://doi.org/10.1016/j.jnoncrysol.2009.08.038>.
14
15

16
17 (13) García-González, C. A.; López-Iglesias, C.; Concheiro, A.; Alvarez-Lorenzo, C. Chapter
18 16. Biomedical Applications of Polysaccharide and Protein Based Aerogels. In *Green Chemistry*
19 *Series*; Thomas, S., Pothan, L. A., Mavelil-Sam, R., Eds.; Royal Society of Chemistry:
20 Cambridge, 2018; pp 295–323. <https://doi.org/10.1039/9781782629979-00295>.
21
22
23

24
25 (14) Silva, G. A.; Coutinho, O. P.; Ducheyne, P.; Shapiro, I. M.; Reis, R. L. The Effect of
26 Starch and Starch-Bioactive Glass Composite Microparticles on the Adhesion and Expression of
27 the Osteoblastic Phenotype of a Bone Cell Line. *Biomaterials* **2007**, *28* (2), 326–334.
28
29 <https://doi.org/10.1016/j.biomaterials.2006.07.009>.
30
31
32

33
34 (15) Zhang, R.; Ma, P. X. Synthetic Nano-Fibrillar Extracellular Matrices with Predesigned
35 Macroporous Architectures. *J. Biomed. Mater. Res.* **2000**, *52* (2), 430–438.
36
37

38
39 (16) Reverchon, E.; Cardea, S.; Rapuano, C. A New Supercritical Fluid-Based Process to
40 Produce Scaffolds for Tissue Replacement. *The Journal of Supercritical Fluids* **2008**, *45* (3),
41
42 365–373. <https://doi.org/10.1016/j.supflu.2008.01.005>.
43
44

45
46 (17) Baldino, L.; Naddeo, F.; Cardea, S.; Naddeo, A.; Reverchon, E. FEM Modeling of the
47 Reinforcement Mechanism of Hydroxyapatite in PLLA Scaffolds Produced by Supercritical
48
49
50

1
2
3 Drying, for Tissue Engineering Applications. *Journal of the Mechanical Behavior of Biomedical*
4 *Materials* **2015**, *51*, 225–236. <https://doi.org/10.1016/j.jmbbm.2015.07.021>.
5
6

7
8 (18) Ma, Z.; Gao, C.; Gong, Y.; Shen, J. Paraffin Spheres as Porogen to Fabricate Poly(L-
9 Lactic Acid) Scaffolds with Improved Cytocompatibility for Cartilage Tissue Engineering.
10 *Journal of Biomedical Materials Research* **2003**, *67B* (1), 610–617.
11 <https://doi.org/10.1002/jbm.b.10049>.
12
13
14
15

16
17 (19) *Modern Pharmaceutics*, 4th ed., rev.expanded.; Banker, G. S., Rhodes, C. T., Eds.; Drugs
18 and the pharmaceutical sciences; Marcel Dekker: New York, 2002.
19
20
21
22

23
24 (20) Wang, H.; Gong, S.; Lin, Z.; Fu, J.; Xue, S.; Huang, J.; Wang, J. In Vivo
25 Biocompatibility and Mechanical Properties of Porous Zein Scaffolds. *Biomaterials* **2007**, *28*
26 (27), 3952–3964. <https://doi.org/10.1016/j.biomaterials.2007.05.017>.
27
28
29
30

31 (21) Tu, J.; Wang, H.; Li, H.; Dai, K.; Wang, J.; Zhang, X. The in Vivo Bone Formation by
32 Mesenchymal Stem Cells in Zein Scaffolds. *Biomaterials* **2009**, *30* (26), 4369–4376.
33 <https://doi.org/10.1016/j.biomaterials.2009.04.054>.
34
35
36
37

38 (22) Kommanaboyina, B.; Rhodes, C. T. Trends in Stability Testing, with Emphasis on
39 Stability During Distribution and Storage. *Drug Development and Industrial Pharmacy* **1999**, *25*
40 (7), 857–868. <https://doi.org/10.1081/DDC-100102246>.
41
42
43
44
45

46 (23) Santos-Rosales, V.; Ardao, I.; Alvarez-Lorenzo, C.; Ribeiro, N.; Oliveira, A.; García-
47 González, C. Sterile and Dual-Porous Aerogels Scaffolds Obtained through a Multistep
48 Supercritical CO₂-Based Approach. *Molecules* **2019**, *24* (5), 871.
49 <https://doi.org/10.3390/molecules24050871>.
50
51
52
53
54
55

1
2
3 (24) Wilson, R. E. Humidity Control by Means of Sulfuric Acid Solutions, with Critical
4 Compilation of Vapor Pressure Data. *Journal of Industrial & Engineering Chemistry* **1921**, *13*
5
6 (4), 326–331. <https://doi.org/10.1021/ie50136a022>.
7
8

9
10 (25) Wang, S.; Li, C.; Copeland, L.; Niu, Q.; Wang, S. Starch Retrogradation: A
11 Comprehensive Review: Starch Retrogradation.... *Comprehensive Reviews in Food Science and*
12 *Food Safety* **2015**, *14* (5), 568–585. <https://doi.org/10.1111/1541-4337.12143>.
13
14
15

16 (26) García-González, C. A.; Smirnova, I. Use of Supercritical Fluid Technology for the
17 Production of Tailor-Made Aerogel Particles for Delivery Systems. *The Journal of Supercritical*
18 *Fluids* **2013**, *79*, 152–158. <https://doi.org/10.1016/j.supflu.2013.03.001>.
19
20
21
22

23 (27) Druel, L.; Bardl, R.; Vorweg, W.; Budtova, T. Starch Aerogels: A Member of the
24 Family of Thermal Superinsulating Materials. *Biomacromolecules* **2017**, *18* (12), 4232–4239.
25
26
27
28
29
30
31
32
33 <https://doi.org/10.1021/acs.biomac.7b01272>.

34 (28) Ma, P. X. Scaffolds for Tissue Fabrication. *Materials Today* **2004**, *7* (5), 30–40.
35
36
37
38
39
40
41
42
43
44
45
46
47
48
49
50
51
52
53
54
55
56
57
58
59
60 [https://doi.org/10.1016/S1369-7021\(04\)00233-0](https://doi.org/10.1016/S1369-7021(04)00233-0).

(29) García-González, C. A.; Uy, J. J.; Alnaief, M.; Smirnova, I. Preparation of Tailor-Made
Starch-Based Aerogel Microspheres by the Emulsion-Gelation Method. *Carbohydrate Polymers*
2012, *88* (4), 1378–1386. <https://doi.org/10.1016/j.carbpol.2012.02.023>.

(30) Rudaz, C.; Courson, R.; Bonnet, L.; Calas-Etienne, S.; Sallée, H.; Budtova, T.
Aeropectin: Fully Biomass-Based Mechanically Strong and Thermal Superinsulating Aerogel.
Biomacromolecules **2014**, *15* (6), 2188–2195. <https://doi.org/10.1021/bm500345u>.

1
2
3 (31) Budtova, T. Cellulose II Aerogels: A Review. *Cellulose* **2019**, *26* (1), 81–121.
4
5 <https://doi.org/10.1007/s10570-018-2189-1>.
6
7

8 (32) Miao, Z.; Ding, K.; Wu, T.; Liu, Z.; Han, B.; An, G.; Miao, S.; Yang, G. Fabrication of
9 3D-Networks of Native Starch and Their Application to Produce Porous Inorganic Oxide
10 Networks through a Supercritical Route. *Microporous and Mesoporous Materials* **2008**, *111* (1–
11 3), 104–109. <https://doi.org/10.1016/j.micromeso.2007.07.018>.
12
13
14
15
16
17

18 (33) Cabra, V.; Arreguin, R.; Vazquez-Duhalt, R.; Farres, A. Effect of Temperature and PH
19 on the Secondary Structure and Processes of Oligomerization of 19 KDa Alpha-Zein. *Biochimica*
20 *et Biophysica Acta (BBA) - Proteins and Proteomics* **2006**, *1764* (6), 1110–1118.
21 <https://doi.org/10.1016/j.bbapap.2006.04.002>.
22
23
24
25
26
27

28 (34) Sun, C.; Dai, L.; Liu, F.; Gao, Y. Simultaneous Treatment of Heat and High Pressure
29 Homogenization of Zein in Ethanol–Water Solution: Physical, Structural, Thermal and
30 Morphological Characteristics. *Innovative Food Science & Emerging Technologies* **2016**, *34*,
31 161–170. <https://doi.org/10.1016/j.ifset.2016.01.016>.
32
33
34
35
36
37

38 (35) Zhang, J.; Wen, C.; Zhang, H.; Zandile, M.; Luo, X.; Duan, Y.; Ma, H. Structure of the
39 Zein Protein as Treated with Subcritical Water. *International Journal of Food Properties* **2018**,
40 *21* (1), 128–138. <https://doi.org/10.1080/10942912.2017.1414839>.
41
42
43
44
45

46 (36) Shukla, R.; Cheryan, M. Zein: The Industrial Protein from Corn. *Industrial Crops and*
47 *Products* **2001**, *13* (3), 171–192. [https://doi.org/10.1016/S0926-6690\(00\)00064-9](https://doi.org/10.1016/S0926-6690(00)00064-9).
48
49
50
51
52
53
54
55
56
57
58
59
60

1
2
3 (37) Pascoli, M.; de Lima, R.; Fraceto, L. F. Zein Nanoparticles and Strategies to Improve
4 Colloidal Stability: A Mini-Review. *Frontiers in Chemistry* **2018**, *6*.
5
6 <https://doi.org/10.3389/fchem.2018.00006>.
7
8

9
10 (38) Gibson, L. J.; Ashby, M. F. *Cellular Solids: Structure and Properties*, 2nd ed.;
11 Cambridge University Press, 1997. <https://doi.org/10.1017/CBO9781139878326>.
12
13

14
15 (39) Groß, J.; Fricke, J. Scaling of Elastic Properties in Highly Porous Nanostructured
16 Aerogels. *Nanostructured Materials* **1995**, *6* (5–8), 905–908. <https://doi.org/10.1016/0965->
17
18
19
20
21
22
23 9773(95)00206-5.

24 (40) Rege, A.; Schestakow, M.; Karadagli, I.; Ratke, L.; Itskov, M. Micro-Mechanical
25 Modelling of Cellulose Aerogels from Molten Salt Hydrates. *Soft Matter* **2016**, *12* (34), 7079–
26
27
28
29
30
31 7088. <https://doi.org/10.1039/C6SM01460G>.

32 (41) Karadagli, I.; Schulz, B.; Schestakow, M.; Milow, B.; Gries, T.; Ratke, L. Production of
33 Porous Cellulose Aerogel Fibers by an Extrusion Process. *The Journal of Supercritical Fluids*
34
35
36
37
38
39
40
41
42
43
44
45
46
47
48
49
50
51
52
53
54
55
56
57
58
59
60
2015, *106*, 105–114. <https://doi.org/10.1016/j.supflu.2015.06.011>.

(42) Plappert, S. F.; Nedelec, J.-M.; Rennhofer, H.; Lichtenegger, H. C.; Liebner, F. W. Strain
Hardening and Pore Size Harmonization by Uniaxial Densification: A Facile Approach toward
Superinsulating Aerogels from Nematic Nanofibrillated 2,3-Dicarboxyl Cellulose. *Chemistry of
Materials* **2017**, *29* (16), 6630–6641. <https://doi.org/10.1021/acs.chemmater.7b00787>.

(43) Zhao, S.; Malfait, W. J.; Guerrero-Alburquerque, N.; Koebel, M. M.; Nyström, G.
Biopolymer Aerogels and Foams: Chemistry, Properties, and Applications. *Angewandte Chemie
International Edition* **2018**, *57* (26), 7580–7608. <https://doi.org/10.1002/anie.201709014>.

1
2
3 (44) Rege, A.; Ratke, L.; Itskov, M. Chapter 8. Modelling and Simulations of Polysaccharide
4 and Protein Based Aerogels. In *Green Chemistry Series*; Thomas, S., Pothan, L. A., Mavelil-
5 Sam, R., Eds.; Royal Society of Chemistry: Cambridge, 2018; pp 129–150.
6
7
8
9
10 <https://doi.org/10.1039/9781782629979-00129>.

11
12
13 (45) Buchtová, N.; Pradille, C.; Bouvard, J.-L.; Budtova, T. Mechanical Properties of
14 Cellulose Aerogels and Cryogels. *Soft Matter* **2019**, *15* (39), 7901–7908.
15
16
17
18 <https://doi.org/10.1039/C9SM01028A>.

19
20
21 (46) Ganesan, K.; Barowski, A.; Ratke, L.; Milow, B. Influence of Hierarchical Porous
22 Structures on the Mechanical Properties of Cellulose Aerogels. *Journal of Sol-Gel Science and*
23 *Technology* **2019**, *89* (1), 156–165. <https://doi.org/10.1007/s10971-018-4828-2>.

24
25
26 (47) Goimil, L.; Jaeger, P.; Ardao, I.; Gómez-Amoza, J. L.; Concheiro, A.; Alvarez-Lorenzo,
27 C.; García-González, C. A. Preparation and Stability of Dexamethasone-Loaded Polymeric
28 Scaffolds for Bone Regeneration Processed by Compressed CO₂ Foaming. *Journal of CO₂*
29 *Utilization* **2018**, *24*, 89–98. <https://doi.org/10.1016/j.jcou.2017.12.012>.

30
31
32 (48) Alcázar-Alay, S. C.; Meireles, M. A. A. Physicochemical Properties, Modifications and
33 Applications of Starches from Different Botanical Sources. *Food Science and Technology*
34 *(Campinas)* **2015**, *35* (2), 215–236. <https://doi.org/10.1590/1678-457X.6749>.

35
36
37 (49) Savich, I. M. Hydrophobic Properties of Maize Zein. *Chemistry of Natural Compounds*
38
39
40
41
42
43
44
45
46
47
48
49 **1991**, *27* (1), 92–95. <https://doi.org/10.1007/BF00629841>.

1
2
3 (50) Rege, A.; Hillgärtner, M.; Itskov, M. Mechanics of Biopolymer Aerogels Based on
4 Microstructures Generated from 2-d Voronoi Tessellations. *The Journal of Supercritical Fluids*
5
6
7
8 **2019**, *151*, 24–29. <https://doi.org/10.1016/j.supflu.2019.04.018>.
9
10
11
12
13
14
15
16
17
18
19
20
21
22
23
24
25
26
27
28
29
30
31
32
33
34
35
36
37
38
39
40
41
42
43
44
45
46
47
48
49
50
51
52
53
54
55
56
57
58
59
60